PHYSICAL REVIEW E **91**, 060501(R) (2015)

Asymmetric counterpropagating fronts without flow

I. Andrade-Silva,[1] M. G. Clerc,[1] and V. Odent[1,2]

[1]*Departamento de Física, Facultad de Ciencias Físicas y Matemáticas, Universidad de Chile, Casilla 487-3, Santiago, Chile*

[2]*Université Lille 1, Laboratoire de Physique des Lasers, Atomes et Molécules, CNRS UMR8523. 59655 Villeneuve d'Ascq Cedex, France*

(Received 8 January 2015; published 15 June 2015)

Out-of-equilibrium systems exhibit domain walls between different states. These walls, depending on the type of connected states, can display rich spatiotemporal dynamics. In this Rapid Communication, we investigate the asymmetrical counterpropagation of fronts in an in-plane-switching cell filled with a nematic liquid crystal. Experimentally, we characterize the different front shapes and propagation speeds. These fronts present dissimilar elastic deformations that are responsible for their asymmetric speeds. Theoretically, using a phenomenological model, we describe the observed dynamics with fair agreement.

DOI: 10.1103/PhysRevE.91.060501 PACS number(s): 61.30.Gd, 42.15.Dp, 05.45.−a, 73.20.Hb

Macroscopic systems influenced by injection and dissipation of energy and/or matter typically exhibit coexistence of different stable states—this feature is usually denominated multistability [1–3]. Heterogeneous initial conditions caused by inherent fluctuations generate spatial domains, which are separated by interfacial domain walls. These interfaces are known as front interfaces or domain walls [2,3]. Interfaces between these metastable states appear in the form of propagating fronts and give rise to a rich spatiotemporal dynamic [4–6]. Front dynamics have been observed in several contexts, such as walls separating magnetic domains [7], directed solidification processes [8], nematic liquid crystals [9], oscillating chemical reactions [10], and fluidized granular media [11], among others. According to the dynamical system theory, in one spatial dimension, a front is a nonlinear solution that is identified in the comoving frame system as a heteroclinic orbit linking two spatially extended uniform states [12]. The front solutions can be regarded as a particle type, i.e., they can be characterized by a set of continuous parameters such as position, core width, and so forth. The front propagation depends on the nature of the states that are being connected. For example, in the case of a front connecting a stable and an unstable state, its speed is not unique but determined by the initial conditions [13]. This scenario changes for a front connecting two stable uniform states. For variational systems, the most stable state invades the other one in order to minimize its nonequilibrium energy or Lyapunov functional; in this sense, the front is always propagating towards the higher energy state [6]. There is only one point in the parameter space for which the front is motionless. Commonly called Maxwell's point, it is the point for which both connected states have exactly the same energy [14]; close to this point, based on variational methods, one can analytically determine the front speed. Furthermore, far from Maxwell's point, implicit expressions for the front speed can be obtained for variational systems [6], through the solution of the corresponding nonlinear eigenvalue problem.

In a bistable isotropic system, one expects that two counterpropagating fronts with the same speed can be created though a finite perturbation over the less favorable state, thus making the most stable state to emerge. Notwithstanding, we have observed that perturbations of an Ising type walls in nematic liquid crystals with reflection symmetry generate two asymmetric counterpropagating fronts, each with a different speed and shape (see Fig. 1). The perturbations are generated by the presence of glass spheres inside the liquid crystal sample. The dynamical behavior observed is common in systems under the influence of an external flow, i.e., drifting or convective systems [15]. In such case, the front that propagates in the drag force direction spreads faster than the one which propagates in the opposite direction. Likewise, the speed difference between the fronts accounts for the drag force. In addition, anisotropic propagation of defects with opposite topological charges has been reported in liquid crystals [16–18]. In this case the asymmetry of the propagation is due to the backflow around moving defects.

In this Rapid Communication, we investigate the counterpropagation of asymmetrical fronts connecting different molecular-orientation configurations in an in-plane-switching cell filled with a nematic liquid crystal without a flow. These fronts are triggered by the presence of glass bead within the sample. Experimentally, we characterize the profile and the speed of these fronts with respect to the voltage applied to the liquid crystal cell. Based on the liquid-crystal molecular orientation induced by the glass bead, we elucidate that the fronts generated by these spheres have different elastic deformations at the core of the fronts. These deformations are responsible for the asymmetry in the shape and speed of the fronts. We propose a simple phenomenological equation—a bistable model under the influence of a nonlinear gradient—to describe the asymmetric counterpropagating fronts without flow. Analytically, we characterize the shape and the speed of the asymmetric counterpropagating fronts which qualitatively describes the observed dynamics.

Experimental setup. To investigate the front propagation we have considered an in-plane-switching cell filled with a nematic liquid crystal. The experimental setup under study is depicted in Fig. 2. A layer of $E7$ nematic liquid crystal is inserted between two glass plates, thickness $g = 1$ mm, with a cell gap $d = 8.8 \pm 0.2$ μm. The elastic constants of the liquid crystal under consideration are $K_1 = 11.2$, $K_2 = 6.8$, and $K_3 = 18.6$ ($\times 10^{-12}$ N). The perpendicular and parallel dielectric constants are $\epsilon_\perp = 5.16$ and $\epsilon_\parallel = 18.96$, respectively [19–22]. We consider an in-plane-switching cell, with an homogeneous planar alignment (following y axis, cf. Fig. 2) and a perpendicular rubbing to the electric field (Instec, IPS02A88uX00). The indium tin oxide (ITO) electrode width

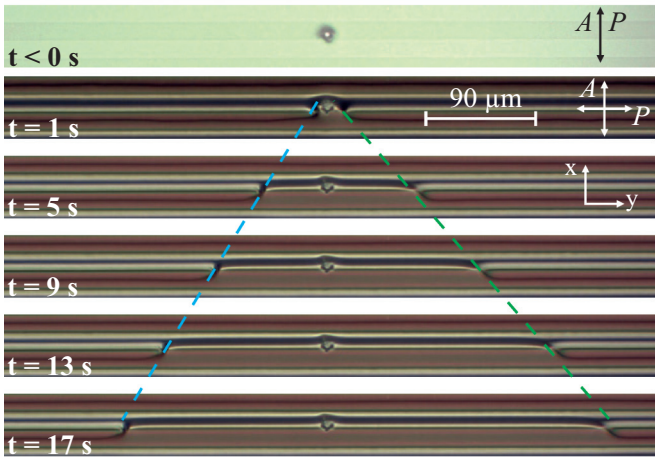

FIG. 1. (Color online) Asymmetric counter propagating fronts in an in-plane-switching cell filled with an $E7$ nematic liquid crystal, applying a tension of $V = 20$ Vpp and $f = 1$ kHz. Experimental snapshots at different times. Parallel polarizer and analyzer (following the x axis) for $t < 0$ and crossed polarizer (following the y axis) and analyzer (following the x axis) for $t > 0$. The black disk in the center is a glass sphere and the dashed lines emphasize the speed with which each front propagates.

and the gap width are the same, $e = 15$ μm. The height of the electrodes is negligible (∼25 nm) compared to the cell thickness ($d = 8.8$ μm). The active zone is a square of side $l = 1$ cm. Under these settings, we can consider the cell in a good approximation as an infinite media in the transverse directions. The electrodes are aligned in the direction of the

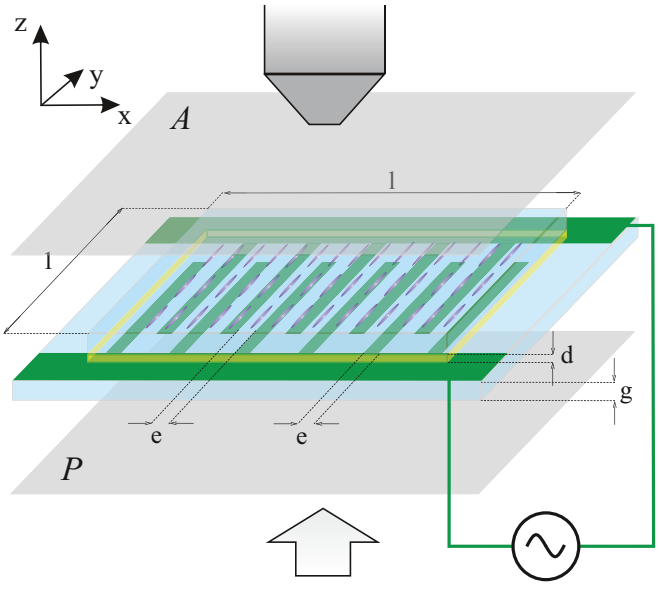

FIG. 2. (Color online) Sketch of the experimental setup, which represents an in-plane-switching cell connected to the functions generator and observed through a microscope (top) with white light (down). Thickness between the two glass plates, $d = 8.8 \pm 0.2$ μm. Thickness of a glass plate, $g = 1$ mm. Active zone, $l \times l = 1$ cm^2. Gap between two electrodes, $e = 15$ μm. The polarizer P and the analyzer A can be either perpendicular or parallel to each other.

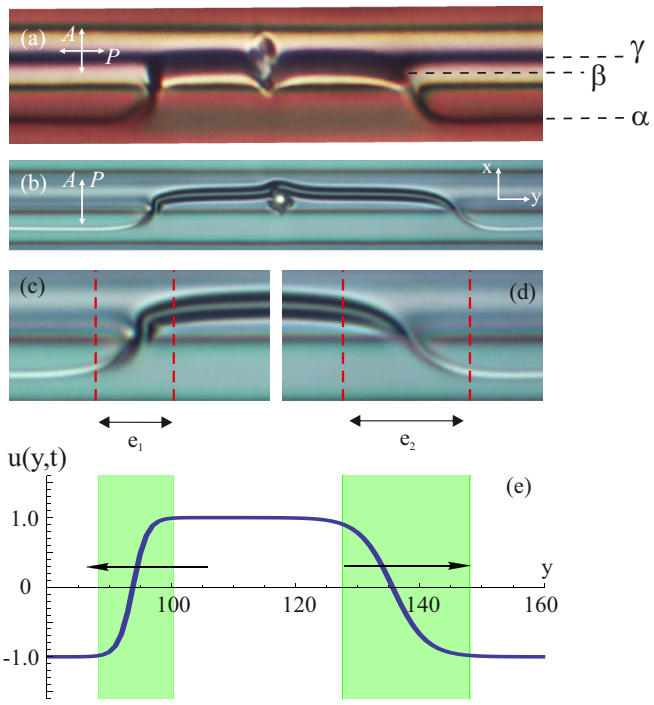

FIG. 3. (Color online) Front profiles. Counterpropagative fronts connecting two different molecular orientations, the α and β states, (a) with a top glass bead perturbation, observed between crossed polarizers, and (b) with a bottom glass bead perturbation, observed between parallel polarizers. (c) Left and (d) right front core with sizes e_1 and e_2, respectively. (e) Stationary solution of model Eq. (1) for $\eta = 0$ and $\nu > 0$.

y axis, that is, the molecules are anchored parallel to the electrodes (see Fig. 2). The electrodes are connected to a function generator that applies an alternating current voltage with frequency ∼10 Hz–100 kHz and amplitude ∼8–20 Vpp. The cell is illuminated with a white light placed between polarizers P and A. In order to have better information about the molecular orientation, the polarizers can be placed either parallel (//) or perpendicular (⊥) to each other. The microscope magnification used is 20× or 50×. The liquid crystal dynamics is measured and recorded through a charge-coupled device (CCD) camera connected to a microscope.

Fronts propagation. Using a CCD camera, we observe in the middle of the sample a small portion of the cell. This midplane is schematically depicted in Fig. 5(e). By direct observation, without applying a voltage to the sample, only the electrode bands can be detected. The top panel in Fig. 1 shows these electrode bands characterized by darker zones. Note that there is a black bead between two consecutive electrodes. This bead is a glass sphere used to fix the thickness between the two glass plates. The glass sphere creates a 3D local perturbation in the molecules orientation around it. Applying a voltage with an amplitude of 20 Vpp with a frequency, $f = 1$ kHz, the system exhibits two asymmetric fronts which propagate on both sides of the glass sphere, following the y axis (cf. Fig. 1). These fronts connect two different molecular orientations, which correspond to black bands observed over the electrodes and between them. Figures 1 and 3 illustrate the front profiles. The black curves are a consequence of the molecular orientations

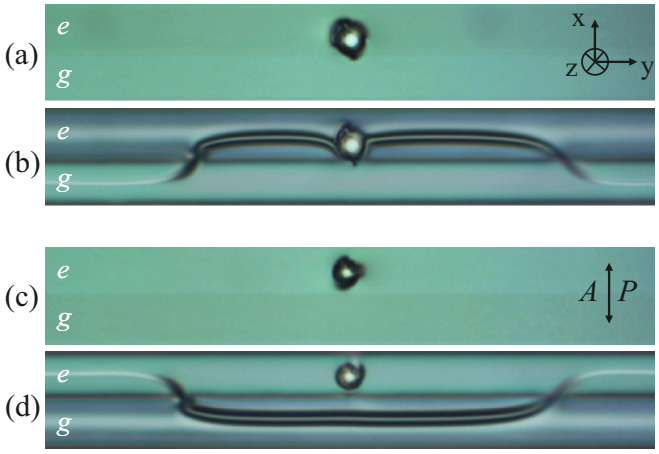

FIG. 4. (Color online) Counterpropagative fronts connecting two different molecular orientations for two different glass bead positions: [(a) and (b)] on an electrode and [(c) and (d)] on a gap. The electrodes and the gap are respectively represented by $\{e,g\}$.

that do not allow the light to cross the sample. As a result of the electrode shapes, the states that connect the fronts are not uniform. Between the gap and the middle electrode, the system exhibits three equilibria, which are represented by α, β, and γ in Fig. 3(a), thanks to the use of crossed polarizers. The fronts only connect two particular molecular orientations. One is positioned in the center of the gap region [α state, see Fig. 3(a)] and the other one is close to the center of the electrode (β state). Then all possible fronts observed from a single glass bead are illustrated in Fig. 4. Notice that at the center of the electrodes, the system presents a peculiar molecular orientation γ state. These states account for a molecular orientation with a certain preferential vertical and horizontal direction, as illustrated in Fig. 5(d). The most stable molecular orientation (the β state) invades the least favorable one (the α state, cf. Fig. 1). Indeed, the states over the electrodes are more stable than those between them. To study the front dynamics, we recorded a video of the front propagation around the glass sphere. We choose a region of the sample where there was only one glass sphere and fix our reference system centered in it. We present a sequence of snapshots at 4-s intervals, where $t = 0\,s$ corresponds to the time where the voltage is applied (cf. Fig. 1). The emerging fronts propagate with a constant speed, nevertheless with different velocities. The left front propagates slower than the right one. The dashed lines in Fig. 1 emphasize this feature. Notice that without the local perturbation induced by the glass sphere, it is difficult to destabilize the first molecular orientation in favor of the second one and so to connect them with a front. One other possibility is to generate these fronts from the electrode tips. The molecular orientations and the fronts are the result of the transverse inhomonogeneous periodic electric field induced by the in-plane switching electrodes [23]. In the bulk of the

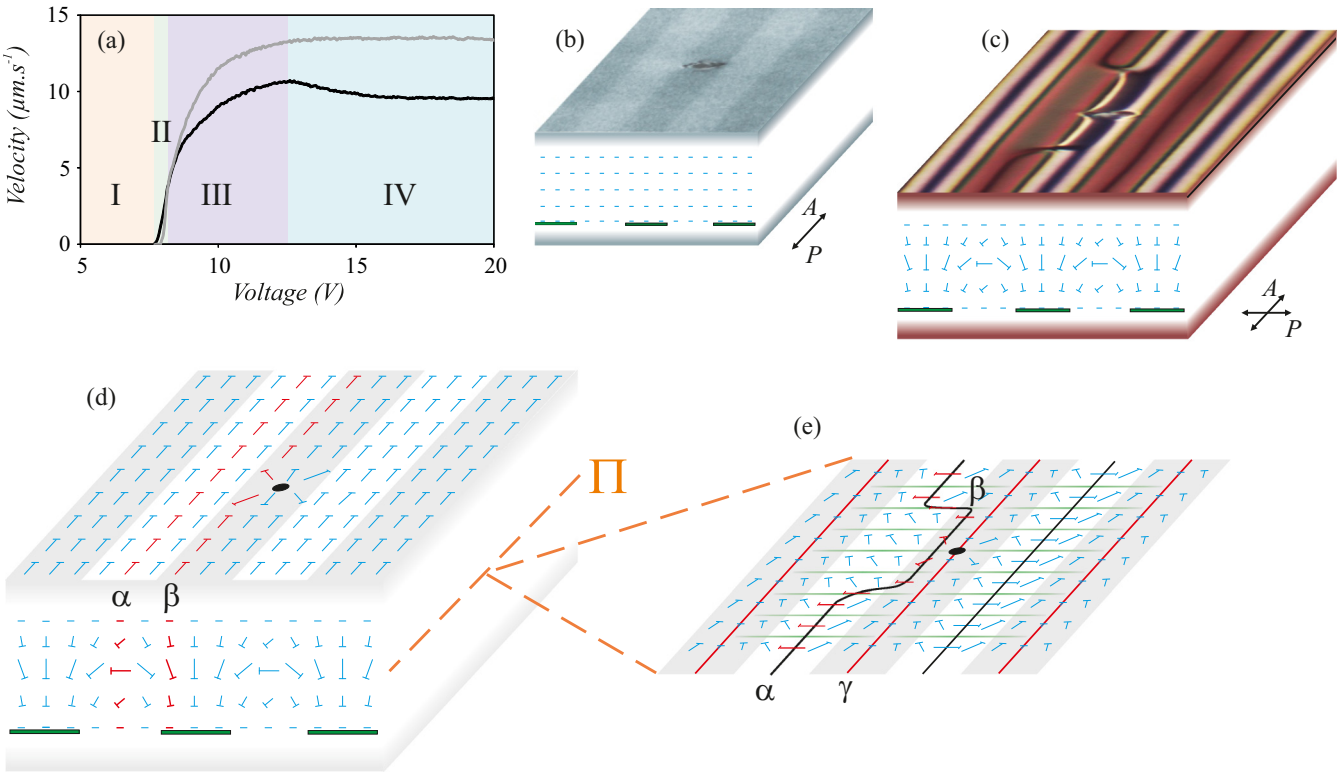

FIG. 5. (Color online) Front solution in an in-plane-switching cell filled with nematic liquid crystal. (a) Left and right front velocity versus voltage amplitude at $f = 1$ kHz; the right and left fronts are represented by gray and black curves, respectively. Experimental snapshots on the top of the sample, (b) without voltage, observed with parallel polarizers ($P//A$), and (c) with voltage, observed between crossed polarizers ($P \perp A$), grayscale image. Schematic molecules orientation in the liquid crystal sample with voltage in the bulk (d) and at the midplane Π (e). The different states that connect the fronts are emphasized in thicker symbols (red) in the bottom panels. • Glass ball causing a local perturbation. Solid lines account for the different walls between domains in panel (e).

sample, the molecules are oriented accordingly to the electric field. The electric field generates walls separating different molecular orientations, particularly walls over and between the electrodes (cf. Fig. 5).

To characterize the front shapes, we have represented the two fronts at $t = 5$ s, with parallel polarizers, $P//A$ [see Fig. 3(b)]. Considering the anchoring conditions and the form of electric field inside the sample, one can infer that the molecules are oriented following mainly the x axis or the y axis. A schematic representation of the molecular orientation with or without tension is shown in Fig. 5. Notice that the fronts do not have the same core sizes (cf. Fig. 3). The core of the front is defined as the transition region between the two asymptotic states. The central location of the front core realizes the front position. The left front, which propagates slower that the right one, has a core size, e_1, smaller than the front core on the right side, e_2. A simple explanation of the origin of the asymmetry between the front cores is as follows: Each core separates different molecular orientations, whereby in the left front the directors rotate clockwise and in the right front they rotate counterclockwise [cf. Fig. 5(e)]. Therefore, as a result of the anisotropic properties of the nematic liquid crystal (i.e., elastic constants [19–22]), they, unlike front cores, generate molecular configurations with different twisting energy. Moreover, it is also expected that the director rotation is coupled with the velocity field to generate an asymmetric backflow [19–22]. These effects are responsible for the dissimilar propagation speeds.

Figure 5(a) shows the front speeds versus the voltage for a fix value of the frequency, $f = 1$ kHz. Experimentally, we observed qualitatively four different regions. In the region of low voltage, corresponding at $V_0 \lesssim 8$ Vpp, the tension is not enough to induce the molecular reorientations, i.e., the system does not exhibit other orientations than those induced by the anchoring conditions. Hence, in this region we do not observe fronts. For $V_0 \simeq 8$ Vpp (region II), we have observed the emergence of fronts. Each front separates different molecular orientation states. The counterpropagative fronts spread with almost the same speed ($v_{\text{front}} < 5$ μm/s). The left front is slightly faster than the right one. In region III, between $V_0 \simeq 9$ Vpp and $V_0 \simeq 12.5$ Vpp, we observe a significant increment of the front speed values. The right front propagates faster than the left one. In the region IV, for $V_0 \gtrsim 12.5$ Vpp, the system exhibits a stationary behavior for counterpropagative fronts. The right and left front speed are constant [$v_{\text{front}}(\text{right}) \approx 13.5$ μm/s and $v_{\text{front}}(\text{left}) \approx 9.5$ μm/s].

Phenomenological description. To study asymmetric counterpropagating one-dimensional fronts that connects the α and β states, let us introduce the following bistable model under the influence of a nonlinear gradient:

$$\partial_t u = \eta + u - u^3 + \partial_{yy} u + \nu u \partial_y u, \tag{1}$$

where $u(y,t)$ is the order parameter [24], which accounts for the front separating the different molecular configurations, and $\{\eta,\ \nu\}$ are parameters which respectively control the relative stability of the states and the asymmetry effects. Note that changing the sign of ν is equivalent to doing the transformation $y \to -y$, so we set $\nu > 0$ without loss of generality. The above model describes an extended imperfect pitchfork bifurcation [2,3], under the influence of a Burgers drift, which is proportional to ν. This term can be taken into account for the asymmetric elastic deformations and the backflow induced to connect the different molecular configurations.

At the Maxwell's point and without Burgers drift, $\eta = \nu = 0$, this model has an unstable homogeneous state $u = 0$ and two stable homogeneous ones, $u_\pm = \pm 1$. This model has motionless fronts of the form $u_{\leftrightarrows}(y) \equiv \pm \tanh[(y - y_0)/c_{\leftrightarrows}]$, with $c_{\leftrightarrows} = \sqrt{2}$. The solution $u_{\leftarrow}(y, y_0)$ [$u_{\rightarrow}(y, y_0)$] represents a front connecting the states u_- [u_+] with u_+ [u_-] when the y coordinate is incremented. We call these solutions the *left* and *right fronts*. The parameter y_0 denotes the front position. Note that the core sizes are denoted as $c_{\leftrightarrows}$. In order to take into account the effect of the Burgers drift, we use the motionless front as an ansatz in Eq. (1) which is an analytical solution for

$$c_{\leftrightarrows} = \mp \frac{\nu}{2} + \sqrt{\left(\frac{\nu}{2}\right)^2 + 2}. \tag{2}$$

Notice that $c_{\leftarrow} < c_{\rightarrow}$. Hence, the left front core is thinner than the right front one. Figure 3(d) shows these fronts, which show a qualitative agreement with the experimentally observed fronts. When one considers that the asymptotic states have different energies, $\eta > 0$ ($\eta < 0$), the asymmetric fronts moves at different constant speeds, such that the most favorable state, u_+ (u_-), invades the less favorable one u_- (u_+). To obtain analytically the front speed, we consider that $\{\eta, v\}$ are small and use the ansatz $u(x,t) = u_{\leftrightarrows}[y - y_0^{\leftrightarrows}(t)] + w(y,t)$, where the front position $y_0^{\leftrightarrows}(t)$ now evolves in time and $w(y,t)$ stands for a small correction. Introducing the above ansatz in Eq. (1), linearizing in w, and applying a solvability condition, after straightforward calculations, we obtain

$$\frac{dy_0^{\leftrightarrows}}{dt} \simeq \mp \frac{3}{\sqrt{2}}\eta + \frac{3}{8}\eta\nu. \tag{3}$$

The first term on the right-hand side accounts for the energy difference between the states. The last term accounts for the effect of Burgers drift, which clearly shows that the right front (left front) is faster than the left front (right front) for $\eta > 0$ ($\eta < 0$). Hence, the front with wider core is always faster. Numerically, we have a good agreement with the previous analytical result.

In conclusion, we have studied the counterpropagation of asymmetrical fronts connecting different molecular orientations in an in-plane-switching cell filled with nematic liquid crystal without a flow. Experimentally, we have characterized the profile and the speed of these fronts. The fronts generated by the glass bead had different elastic deformations at the front cores. These deformations are responsible for the asymmetry in the shape and the speed of the fronts. Theoretically, we have proposed a phenomenological equation, a bistable model under the influence of a nonlinear gradient, to describe the asymmetric counterpropagating fronts without flow. Analytically, we have characterized the shape and the speed of the fronts, which qualitatively describes the observed dynamics.

Acknowledgments. The authors thank F. Roussel and C. Binet for fruitful discussions and N. Maalouli, M. Wilson, and I. Bordeau for their critical reading of the manuscript.

M.G.C. acknowledges the financial support of FONDECYT Project No. 1150507. V.O. acknowledges the support of the "Région Nord- Pas-de-Calais." This work was partially supported by the Centre National de la Recherche Scientifique (CNRS), the Ministry of Higher Education and Research, the Nord-Pas de Calais Regional Council and European Regional Development Fund (ERDF) through the Contrat de Projets Etat-Région (CPER) 2007-2013, as well as by the Agence Nationale de la Recherche through the LABEX CEMPI project (ANR-11-LABX-0007).

[1] G. Nicolis and I. Prigogine, *Self-Organization in Non Equilibrium Systems* (J. Wiley & Sons, New York, 1977).

[2] L. M. Pismen, *Patterns and Interfaces in Dissipative Dynamics*, Springer Series in Synergetics (Springer, Berlin, 2006).

[3] M. Cross and H. Greenside, *Pattern Formation and Dynamics in Nonequilibrium Systems* (Cambridge University Press, New York, 2009).

[4] J. S. Langer, Rev. Mod. Phys. **52**, 1 (1980).

[5] P. Collet and J. P. Eckman, *Instabilities and Fronts in Extended Systems*, Princeton Series in Physics (Princeton University Press, Princeton, 2014).

[6] Y. Pomeau, Physica D (Amsterdam) **23**, 3 (1986).

[7] A. H. Eschenfelder, *Magnetic Bubble Technology* (Springer, Berlin, 1980).

[8] T. Börzsönyi, S. Akamatsu, and G. Faivre, Phys. Rev. E **80**, 051601 (2009).

[9] M. G. Clerc, S. Residori, and C. S. Riera, Phys. Rev. E **63**, 060701 (2001); M. G. Clerc, T. Nagaya, A. Petrossian, S. Residori, and C. Riera, Eur. Phys. J. D **28**, 435 (2004); S. Residori, A. Petrossian, T. Nagaya, C. Riera, and M. G. Clerc, Physica D **199**, 149 (2004); F. Haudin, R. G. Elías, R. G. Rojas, U. Bortolozzo, M. G. Clerc, and S. Residori, Phys. Rev. Lett. **103**, 128003 (2009); Phys. Rev. E **81**, 056203 (2010).

[10] V. Petrov, Q. Ouyang, and H. L. Swinney, Nature **388**, 655 (1997).

[11] S. Douady, S. Fauve, and C. Laroche, Europhys. Lett. **8**, 621 (1989); F. Melo, P. B. Umbanhowar, and H. L. Swinney, Phys. Rev. Lett. **75**, 3838 (1995); S. J. Moon, M. D. Shattuck, C. Bizon, D. I. Goldman, J. B. Swift, and H. L. Swinney, Phys. Rev. E **65**, 011301 (2001); J. E. Macias, M. G. Clerc, C. Falcon, and M. A. Garcia-Nustes, *ibid.* **88**, 020201 (2013).

[12] W. van Saarloos and P. Hohenberg, Physica D **56**, 303 (1992); P. Coullet, Int. J. Bifurcation Chaos **12**, 2445 (2002).

[13] W. van Saarloos, Phys. Rep. **386**, 29 (2003).

[14] R. E. Goldstein, G. H. Gunaratne, L. Gil, and P. Coullet, Phys. Rev. A **43**, 6700 (1991).

[15] J. M. Chomaz, Phys. Rev. Lett. **69**, 1931 (1992).

[16] C. Blanc, D. Svensek, S. Zumer, and M. Nobili, Phys. Rev. Lett. **95**, 097802 (2005).

[17] A. Bogi, P. Martinot-Lagarde, I. Dozov, and M. Nobili, Phys. Rev. Lett. **89**, 225501 (2002).

[18] I. Dierking, M. Ravnik, E. Lark, J. Healey, G. P. Alexander, and J. M. Yeomans, Phys. Rev. E **85**, 021703 (2012).

[19] P. Oswald and P. Pieranski, *Nematic and Cholesteric Liquid Crystals* (Taylor & Francis, Boca Raton, FL, 2005).

[20] I. C. Khoo, *Liquid Crystals*, 2nd ed. (John Wiley & Sons, New York, 2007).

[21] P. G. de Gennes and J. Prost, *The Physics of Liquid Crystals*, 2nd ed. (Clarendon Press, Oxford, 1993).

[22] S. Chandrasekhar, *Liquid Crystals* (Cambridge University Press, New York, 1992).

[23] I. Andrade-Silva, M. G. Clerc, and V. Odent, Phys. Rev. E **90**, 022504 (2014).

[24] D. Ter Haar, ed., *Collected Papers of LD Landau* (Elsevier, Amsterdam, 2013).